Transition from afterglow to streamer discharge in an atmospheric capacitively coupled micro-plasma jet

Sylvain Iséni, Thalita M C Nishime, Torsten Gerling

Applied Physics Letters ARTICLE

Transition from afterglow to streamer discharge in an atmospheric capacitively coupled micro-plasma jet

Cite as: Appl. Phys. Lett. **125**, 203502 (2024); doi: 10.1063/5.0232114
Submitted: 5 August 2024 · Accepted: 31 October 2024
Published Online: 11 November 2024

Sylvain Iseni,[1,a)] Thalita M. C. Nishime,[2] and Torsten Gerling[2]

AFFILIATIONS

[1]GREMI (Groupe de Recherches sur l'Énergétique des Milieux Ionisés)—UMR7344 CNRS/Université d'Orléans, 14 rue d'Issoudun, 45067 Orléans, France
[2]Leibniz Institute for Plasma Science and Technology (INP), Felix-Hausdorff-Straße 2, 17489 Greifswald, Germany

[a)]**Author to whom correspondence should be addressed:** sylvain.iseni@univ-orleans.fr and sylvain.iseni@cnrs.fr

ABSTRACT

This Letter focuses on the discharge mechanisms of an atmospheric pressure micro-plasma jet optimized for endoscopic applications in biology and medicine. This capacitively coupled plasma (CCP) features a concentric double flow allowing for shielding the Helium or Neon plasma gas with carbon dioxide from the humid ambient air. High-resolution optical emission spectroscopy allows for the analyses of the Stark effect of the He I 492.19 nm and the Hydrogen H_β lines to determine the electric field (EF) and the electron density spatially resolved along the discharge expansion outside the source. EF in Neon at atmospheric pressure was reliably determined with the Stark shift measurement of the weak Ne I line at 515.196 nm. In both gases, the EF diagnostic revealed a steep transition from CCP afterglow to streamer discharge with a magnitude up to 30 kV/cm. This research is a significant step forward in the field of plasma medicine with a plasma source capable of delivering a reactive chemistry with or without an intense EF to the target.

For decades, non-thermal plasmas (NTPs) have been studied and used in a variety of applications ranging from materials processing and thin film deposition to, more recently, the treatment of agricultural products and medical applications.[1] In the emerging field of plasma medicine, the use of NTPs as a medical tool in several experimental and clinical procedures has already been effectively established.[2] Cold plasma not only has been used for the disinfection of oral- and skin-based pathogens and treatment of chronic wounds but has also been investigated as a promising tool against tumor cells when in combination with other conventional methods.[3]

Considering the different application fields, specific requirements concerning the plasma source configuration, electrode geometry, and feed gas are important to be considered. Plasma jets are capable of generating a discharge in open air when flushing the electrode's region with a gas flow and/or enhancing the electric field along the jet axis.[4] This unconstrained discharge allows the treatment of punctual and irregular targets, which is especially attractive for medical applications.[5] However, some applications require a certain flexibility from the plasma source design. The use of plasma for oral or intra-corporeal treatments demands not only an improved flexibility of the plasma jet device but also a rather small dimension and the possibility of operating inside hollow bodies.[6] Several approaches have already been reported in the literature that implement such requirements.[6–10] The micro-plasma jet studied here meets all of the aforementioned criteria and is the first to effectively demonstrate antiviral efficacy under defined safe operating conditions.[6,11,12] It is based on a capacitively coupled configuration and has been initially designed for endoscopic applications.[6] It offers a unique degree of versatility with its capability to switch from one discharge mechanism to another. This is different to the so-called conducting and non-conducting modes while applied to a treated surface.[11,12] Hence, getting deeper insight on the plasma properties from the physics of gas discharge is the main motivation of this work.

Taken as a whole, the geometry of this miniaturized plasma jet reminds of the general concept of atmospheric pressure plasma jet devices.[4] This involves guiding a double flow of an inner—noble—gas shielded by an outer inert gas through an outward-opening tube fitted with a pair of electrodes connected to a generator. The latter initiates the gas breakdown and delivers the energy to maintain the discharge, which expands in the ambient yielding a plasma plume ranging from a

few millimeters to a couple of centimeters. In the following, one will focus mainly on the specific features of this micro-plasma jet, while a detailed description has been documented in Refs. 6, 12, and 13. To form two separated gas channels, two nested flexible PTFE tubes of different diameters are used. The internal PTFE capillary has a diameter of 0.9 mm with a wrapped copper wire on its outer surface. This assembly is placed within the second PTFE tube of 1.5 mm inner diameter. This concentric geometry is realized by ceramic nozzle placed at the outlet of the jet. By pressing the outer tube tightly over the thicker portion of the nozzle, the outer tube is attached to the ceramic nozzle. This thicker portion of the nozzle features several grooves to allow the shielding gas to exit the outer tube while surrounding the inner gas used to ignite the discharge. The inner capillary is fed with 300 sccm (standard cubic centimeter) Helium or Neon—with a purity of 99.999%. The latter flow pattern is shielding from the ambient air by feeding the larger tube with 300 sccm carbon dioxide (CO_2) as previously introduced with the kINPen source.[14] The wrapped copper wires act as high voltage (HV) electrode to ignite the discharge within the inner capillary fed with the noble gas. The electrode is powered to a customized self-tuning HV generator delivering a sinusoidal excitation waveform at 0.467(20) MHz. The HV is modulated with a lower frequency signal at 1.0 kHz and a duty cycle set to 32%. Figure 1 shows the HV and current excitation waveforms measured with the help of a HV probe (P6015A, Tektronix) at the generator output. The total current is obtained by measuring the voltage drop across a shunt resistor (100 Ω) connected to a thin wire placed around the capillary outlet with a 100× voltage probe (model TT-HV-250, Testec). The HV amplitude peak-to-peak is set to (4.5 ± 0.2) kV for Helium and (2.7 ± 0.2) kV for Neon, which is sufficient to induce an electric field above the breakdown field while preventing breakdown in the CO_2 shielding. Conveniently, CO_2 is also used instead of the noble gas to measure the displacement current as shown in Fig. 1. An interesting property of this micro-plasma source is the electrical regime of excitation, which is in the smooth transition range between a high

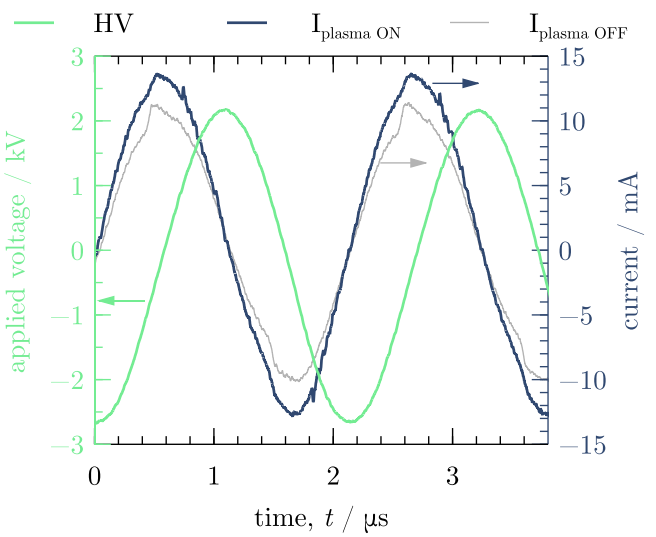

FIG. 1. Time evolution of the measured voltage and current waveforms of the circuit in Helium with and without plasma. $I_{plasma\ OFF}$ corresponds to the displacement current, while the curve $I_{plasma\ ON}$ refers to the total current.

frequency AC excitation and a radio frequency (RF) plasma.[15] In Fig. 1, the current is leading the HV with a phase shift of $(86° \pm 2°)$, which is close to the behavior of an ideal RC circuit. Thus, this micro-plasma jet is electrically operating in a capacitively coupled discharge within the capillary nozzle. With a mean velocity of 40 m/s for a gas flow rate set at 300 sccm, an afterglow is, thus, produced at the exit yielding a thin plasma plume. The rather weak electrical matching between the capacity of the jet head and the generator allows for dissipating a very low power around (150 ± 25) mW (viz., jets 03–04 in Ref. 12).

To get a better insight on the discharge expanding from the jet outlet into the ambient, optical emission spectroscopy (OES) is a method of choice due to its non-intrusive nature. The experimental approach is similar to that used in a previous study,[16] where the entire plasma plume is imaged onto the entrance slit of a spectrograph using a couple of lenses. This makes it possible to record a spectrum at every point in space along the axis of propagation of the plasma plume. The performance is newly improved with the use a double-stage triple grating imaging spectrometer with an effective focal length of 1.5 m (DuoVista DM77, S&I). A 16 bit cryogenic cooled CCD array of 1340×400 pixels (PyLoN, Teledyne Princeton Instruments) is mounted at the exit to capture the spatially resolved spectra. The whole system is able to record the spectra from 200 to 1200 nm with a spectral resolution down to 4 pm depending on the grating, the entrance slit width, and the central wavelength. Spatially resolved OES diagnostics—with a resolution of 15 μm/px and a depth of field equal to 5 mm—is realistic due to the stable experimental conditions and the highly reproducible plasma source.

The electric field (EF) and the electron properties are key features in the physics of non-equilibrium plasmas. Getting access to the EF strength in the discharge will reveal important information on the *governing elementary processes*. In practice, the EF in Helium discharges can be investigated by analyzing the emission line profile of the π-polarized linear Stark splitting and shift with their forbidden counterparts. The advantage of this method—like other Stark methods—is its *ab initio* nature. Several atomic Helium lines can be used to estimate the EF,[17] but they all suffer from a rather low emissivity, making them difficult to observe. For this reason, the allowed He I transition $(4d\,^1D \rightarrow 2p\,^1P^0)$ line at 492.19 nm—with its forbidden transition $(4f\,^1F \rightarrow 2p\,^1P^0)$—is chosen for its reasonable emissivity and its sensitivity to the EF. As demonstrated in Ref. 18, high-resolution space-resolved EF measurements are achieved with time-integrated OES emission recorded during the streamer growth. Several studies found in the literature have demonstrated the consistency of this method to diagnose streamer-based discharges,[19] e.g., DBDs,[20] plasma jets,[18] and cathode sheath.[21,22]

Figure 2 shows the spectral evolution of the He I line at 492.19 nm spatially resolved along the expansion direction of the plasma plume. The main focus is on the central line, $\lambda = \lambda_0$, while the other multiple lines (e.g., $-1\,\text{nm} < \lambda - \lambda_0 < -0.35\,\text{nm}$) correspond to some rotational transitions from highly excited vibrational bands of molecular nitrogen. Note that the emission from the second positive system of N_2 increases within the last millimeter of the plasma plume. This is explained by the efficient action of the shielding gas in the first millimeters from the nozzle to shield the free stream core area from ambient air species diffusion into the plasma plume after 3 mm distance. About the He I line, it is remarkable to observe that its

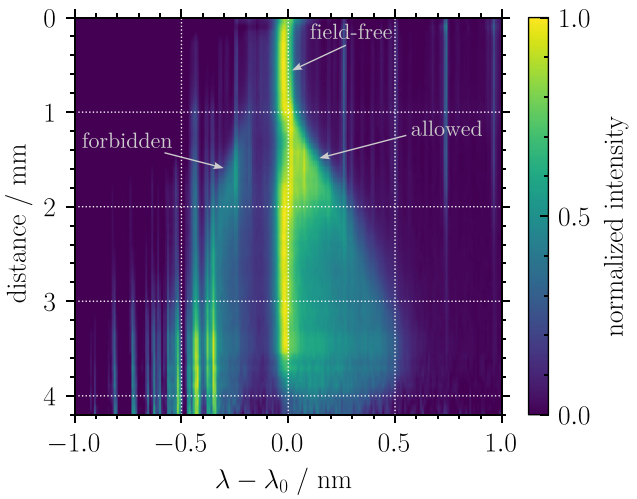

FIG. 2. Spectrally resolved image along the propagation direction of the micro-plasma jet. The nozzle outlet is set to 0.0 mm, and the spectral window is centered on the He I line, $\lambda_0 = 492.19$ nm. The intensity is normalized to the maximum of the spectrum (horizontal axis) recorded at each distance. Integration time: 20 min; collected light: *p*-polarized.

dispersion increases together with the distance position along the plasma plume. Two regions can be identified: from the nozzle exit ranging from 0.0 to 1.0 mm, the optical transition exhibits a single line with a constant broadening due to the Van der Waals interactions with other atoms. Starting at 1.0 mm distance, the second region is characterized with a significantly progressive broadening of the He I line. The dispersion pattern observed in a spectral image made of many individual spectra clearly evidences an evolution of the profile line shape of the He I transition. Qualitatively, the so-called field-free component is in the center (λ_0), and it originates from the plasma volume where the EF is negligible. Its forbidden emitted counterpart is gradually appearing on the left side, but it becomes partly overlapping with the emission of excited N_2 coming from the impurities. In the case of Fig. 2, the most striking characteristic is the shift to the red of the He I line, which is the signature of the Stark effect. The reader may refer to Fig. 3 in Ref. 23 for comprehensive identification of the He I 492.19 nm line shape. Essentially, the Stark effect is the change in energy levels of an emitter exposed to an EF that can result from a strong longitudinal gradient of external field in the discharge or from a high density of charged particles—often electrons. There is no doubt that the electron density (n_e) in atmospheric pressure plasma jets is too low to produce Stark profile of this magnitude.[24] Consequently, the observation of the Stark broadening reveals the presence of a large and monotonically rising longitudinal EF within the second region plasma plume. In other words, the discharge physics and the underlying elementary processes involved in first region (0.0–1.0 mm) are of different nature in the second part starting at 1.0 mm. A quantitative analysis of the spectra shown in Fig. 2 will be discussed later in order to study in more detail the EF profile along the plasma plume.

To ensure that this is not a peculiarity of the He discharge, the micro-plasma jet is then operated with neon gas. This choice is not only motivated by the possible use of this plasma source in medical endoscopic applications[6,11] but also for the opportunity to diagnose the EF by OES. Indeed, Ne gas—like any other atomic element in the gas phase—can have its electronic transition affected by the Stark effect. However, the observation is often unfruitful due to its negligible contribution compared to other broadening mechanisms.[25] Conveniently, Ne I lines Stark effect studies have recently been directed toward lower EF values allowing for suitable diagnostics in non-equilibrium plasma. An in-depth comparison of the Stark shift of numerous Ne I lines with the known π-polarized linear Stark effect of Hydrogen shows remarkable agreement with the measurement of the EF value in the cathodic sheath region of a low-pressure discharge.[26] Nevertheless, the emissivity of the most sensitive Ne I lines to the Stark effect is very weak compared to other emission lines from the discharge, which makes the detection challenging. In the current study, the transition Ne I ($5d\,^2P^\circ[5/2]2 \rightarrow 3p\,^2P^\circ[3/2]1$) at 515.196 nm is the only line that could be observed without any overlapping with the molecular emission bands—of residual impurities from the gas bottle (e.g., N_2). The spectral evolution of the Ne I line spatially resolved along the expansion direction of the plasma plume is shown in Fig. 3. Here again, two regions are identified: The first closer to the nozzle (from 0.0 to 1.8 mm) with a non-shifted Ne I line at $\lambda - \lambda_0 = 0$ nm. The second region starts at 1.8 mm distance from the jet outlet and is characterized by a sudden shift to the red of the Ne I line. This is a clear evidence of the Stark effect resulting from a significant increase in the EF in this second part of the plasma plume. Qualitatively, this reminds of the situation with He gas, which indicates that it is not feed gas dependent—although the separation between the two zones slightly differs in space and can be explained by a longer plume length in Ne than in He. This strong and localized discontinuity indicates a change in the discharge operation. It also means that the elementary processes involved in the ionization to sustain the discharge are different. This motivates a quantitative evaluation of the EF for both gases and the measurement of n_e.

The relation between the Stark shift ($\Delta\lambda$) of the Ne I line and the EF is detailed in Ref. 26 and is also validated in Ref. 27 for values up to 14.55 kV/cm. It reads

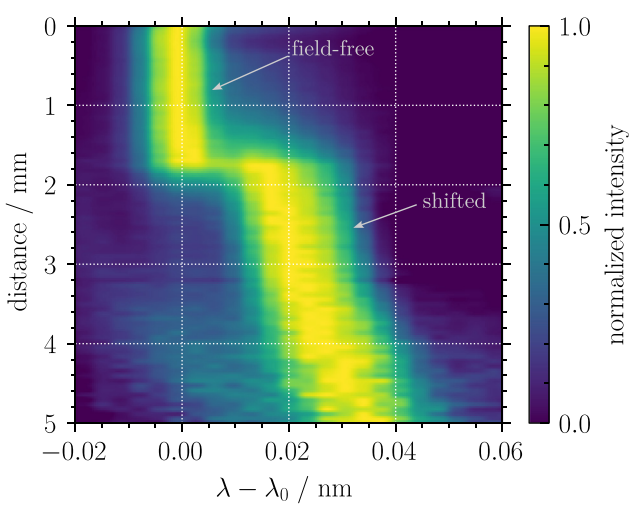

FIG. 3. Spectrally resolved image along the propagation direction of the micro-plasma jet. The nozzle outlet is set to 0.0 mm, and the spectral window is centered on the Ne I line, $\lambda_0 = 515.196$ nm. The intensity is normalized to the maximum of the spectrum (horizontal axis) recorded at each distance. Integration time: 45 min.

$$\Delta\lambda = -(\lambda_0 F)^2 \cdot \kappa, \quad (1)$$

with $\kappa = -22.9 \times 10^{-3}$ cm/kV^2 for the transition λ_0 at 515.196 nm.[26] To analyze the spectra shown in Fig. 3, a line shape model is used to accurately determine values of $\Delta\lambda$. It is described by two Voigt profiles corresponding to the field-free and the shifted lines. An example of the excellent agreement with a recorded spectrum is shown in Fig. 4. The Gaussian contribution to the Voigt profiles corresponds to the instrumental profile—previously characterized. It is fixed to 9 pm. Apart from the transition point around 1.8 mm where both the field-free and the shifted lines emit together in some proportion, only the shifted component is found. In order to keep the position of the field-free component in the model, reference spectra from a low-pressure Ne lamp are previously recorded for each row of the CCD array. This is to correct for the possible optical aberration of the spectrometer, which might artificially shift the line on the edges of the array (i.e., astigmatism) and would affect the value of $\Delta\lambda$.

The spectral line shape of He I shown in Fig. 2 is analyzed according to Ref. 23. A line shape model including the three components of the He I 492.19 nm is computed and adjusted to the experimental data in order to determine the central position of each contribution. Then, the spectral distance between the forbidden and the allowed components is used to determine the EF value according to the well-known formalism reviewed in Ref. 17. The evolution of the EF along the plasma plume is shown in Fig. 5 for both gases. The measurement of n_e is made with the line profile analysis of the Hydrogen Balmer beta line (H_β). An example of the recorded profile is shown together with the fit result of a Voigt distribution—constrained by fixing the instrumental broadening contribution. The model describes the H_β profile over almost three orders of magnitude, which is very convincing when it comes to determining n_e from its full width at half maximum (FWHM). Figure 5 resembles a typical EF dynamic observed in the growth of streamer head in He. The magnitude ranges from 10 to 30 kV/cm, which is in excellent agreement with the values found in the literature of He ionization waves.[18,19,23,24] The streamer initiation is located at 1.0 mm distance for a value of 10 kV/cm, which corresponds

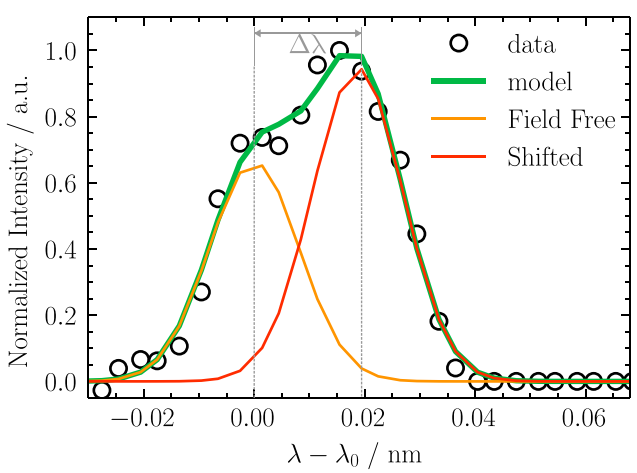

FIG. 4. Comparison of the recorded line shape of the Ne I line at $\lambda_0 = 515.196$ nm with the result of a fitting model. The data correspond to the spectrum recorded at 1.9 mm distance from the nozzle (see Fig. 3).

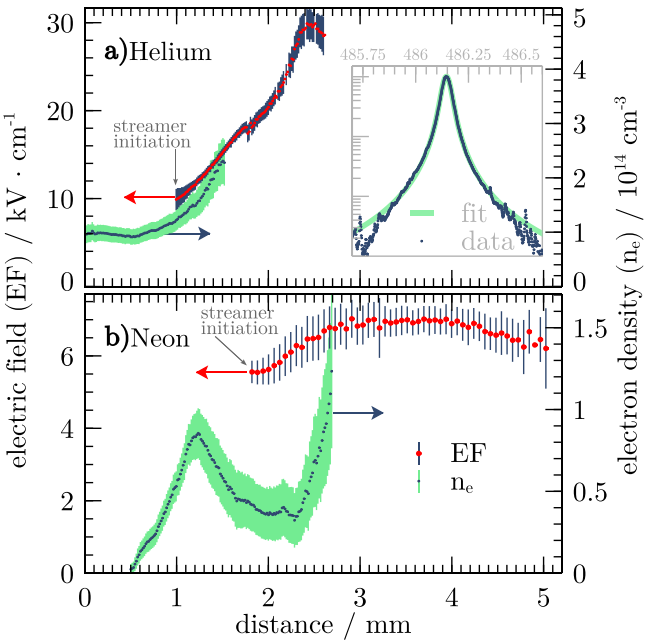

FIG. 5. EF and n_e distributions along the plasma plume with the micro-plasma jet operated in He (a) and Ne (b). The inset plot shows the profile line shape of H_β together with the best fit model.

to the breakdown field of He.[28] It should be noted that an evaluation of the EF beyond the position starting at 2.5 mm was not possible due to the overlapping of the Stark broadened He line by rotational structures, which became relatively important (see Fig. 2). The n_e distribution describes a monotonic trend over the measurement range. This transition is also observed on the axial profile of n_e, which remains constant around 1×10^{14} cm^3 in the afterglow region (0 to 1.0 mm) before a significant enhancement in the streamer part.

A sharp rise of EF is also diagnosed with the micro-plasma jet operating in Ne, with a moderate EF enhancement after the streamer initiation position (1.8 mm), as shown in Fig. 5(b). Interestingly, the EF of the Ne ionization wave is in the range 5.5–7 kV/cm, which is lower than in He. According to the author's best understanding, the literature does not report on EF values in ionization waves in Ne gas. Meanwhile, Ne is known to have a significantly higher ionization rate than He as well as a lower breaking field.[28] This would also support the constant EF profile compared to the He case. Regarding the n_e, it is lower than for the He case. The n_e distribution is not monotonic, with a maximum close to the end of the afterglow region (at 1.2 mm). At the streamer initiation position (1.8 mm), n_e is reduced by half its maximum value. This value of 5×10^{13} cm^3, which, under the current conditions, is sufficient to satisfy the Meek criterion for streamer growth, results in an increase in n_e up to 1×10^{14} cm^3, as observed in the experiment.

In this Letter, a capacitively coupled micro-plasma jet operating in two noble gases, namely, He and Ne, is investigated with regard to the discharge characteristic. By means of advanced OES techniques, the produced plasma plume was diagnosed along its expansion direction. As a key parameter in gas discharge, the induced electric field was effectively measured space-resolved. While the Stark effect in He gas

has been effectively applied in the diagnostics of ionization waves, this work extends the possibility to measure the EF in Ne gas APPJ. The observation and the subsequent analysis of the red-shifted Stark line of Ne I ($5d\,^2P^\circ[5/2]2 \rightarrow 3p\,^2P^\circ[3/2]1$) at 515.196 nm were used to quantify the EF in the Ne streamer head. The localized and strong enhancement of the EF is found in the plasma plume with both gases (i.e., 5.5 to 7 kV/cm in Ne and 10 to 30 kV/cm in He). The self-induced EF of this magnitude in a gas discharge is the evidence of the ionization wave inception and the signature of an abrupt transition from afterglow to streamer growth. In essence, the elementary processes are different in the afterglow and streamer regions. This is obviously reflected in the electron density n_e and the resulting non-equilibrium chemistry. Undoubtedly, this unique feature of the micro-plasma jet opens exciting opportunities for biomedical and medical applications, depending on whether biological matter is exposed to reactive plasma chemistry with or without intense EF.

This research was partly supported by the French National Research Agency (ANR) with the project MIDICODE (ANR-22-CE51-0022-01). This study was also supported by a STSM through PlasTHER (E-COST GRANT-CA20114-06c5b4e8). The device was kindly provided by the project PlasmaPlusCorona funded by the German Federal Ministry of Education and Research (BMBF, Grant No. 03COV06A) via R. Bansemer, S. Bekeschus, and T. von Woedtke. In addition, T.G. and T.M.C.N. appreciate the funding received by the Ministry of Economics, Employment and Health of the state Mecklenburg-Vorpommern (Germany), the European Union through European Regional Development Funds (TBI-V-1-361-VBW-124). This work originates from the collaborative project BARISTAS.

DATA AVAILABILITY

The data that support the findings of this study are available from the corresponding author upon reasonable request.

REFERENCES

[1]I. Adamovich, S. Agarwal, E. Ahedo, L. L. Alves, S. Baalrud, N. Babaeva, A. Bogaerts, A. Bourdon, P. J. Bruggeman, C. Canal, E. H. Choi, S. Coulombe, Z. Donkó, D. B. Graves, S. Hamaguchi, D. Hegemann, M. Hori, H.-H. Kim, G. M. W. Kroesen, M. J. Kushner, A. Laricchiuta, X. Li, T. E. Magin, S. M. Thagard, V. Miller, A. B. Murphy, G. S. Oehrlein, N. Puac, R. M. Sankaran, S. Samukawa, M. Shiratani, M. Šimek, N. Tarasenko, K. Terashima, E. Thomas, Jr., J. Trieschmann, S. Tsikata, M. M. Turner, I. J. van der Walt, M. C. M. van de Sanden, and T. von Woedtke, J. Phys. D **55**, 373001 (2022).
[2]T. V. Woedtke, A. Schmidt, S. Bekeschus, K. Wende, and K.-D. Weltmann, In Vivo **33**, 1011 (2019).
[3]A. Nitsch, S. Qarqash, S. Römer, J. Schoon, D. Singer, S. Bekeschus, A. Ekkernkamp, G. I. Wassilew, M. V. Tzvetkov, and L. Haralambiev, Sci. Rep. **14**, 6505 (2024).
[4]X. Lu, M. Laroussi, and V. Puech, Plasma Sources Sci. Technol. **21**, 034005 (2012).
[5]M. Laroussi, IEEE Trans. Plasma Sci. **43**, 703 (2015).
[6]J. Winter, T. M. Nishime, S. Glitsch, H. Lühder, and K.-D. Weltmann, Contrib. Plasma Phys. **58**, 404 (2018).
[7]A. V. Omran, F. Sohbatzadeh, S. N. Siadati, A. H. Colagar, Y. Akishev, and F. Arefi-Khonsari, J. Phys. D **50**, 315202 (2017).
[8]T. M. C. Nishime, R. Wagner, and K. G. Kostov, Polymers **12**, 1028 (2020).
[9]Y. Binenbaum, G. Ben-David, Z. Gil, Y. Z. Slutsker, M. A. Ryzhkov, J. Felsteiner, Y. E. Krasik, and J. T. Cohen, PLoS One **12**, e0169457 (2017).
[10]M. Kurosawa, T. Takamatsu, H. Kawano, Y. Hayashi, H. Miyahara, S. Ota, A. Okino, and M. Yoshida, J. Surg. Res. **234**, 334 (2019).
[11]D. M. Mrochen, L. Miebach, H. Skowski, R. Bansemer, C. A. Drechsler, U. Hoffmann, M. Hein, U. Mamat, T. Gerling, U. Schaible, T. von Woedtke, and S. Bekeschus, Free Radical Biol. Med. **191**, 105 (2022).
[12]H. Jablonowski, U. Hoffmann, R. Bansemer, S. Bekeschus, T. Gerling, and T. von Woedtke, J. Phys. D **57**, 195202 (2024).
[13]J. Winter, T. M. C. Nishime, R. Bansemer, M. Balazinski, K. Wende, and K.-D. Weltmann, J. Phys. D **52**, 024005 (2019).
[14]S. Bekeschus, S. Iseni, S. Reuter, K. Masur, and K.-D. K. D. Weltmann, IEEE Trans. Plasma Sci. **43**, 776 (2015).
[15]P. Bruggeman and R. Brandenburg, J. Phys. D **46**, 464001 (2013).
[16]S. Iseni, C. Pichard, and A. Khacef, Appl. Phys. Lett. **115**, 034102 (2019).
[17]N. Cvetanović, M. M. Martinović, B. M. Obradović, and M. M. Kuraica, J. Phys. D **48**, 205201 (2015).
[18]A. Sobota, O. Guaitella, G. B. Sretenović, I. B. Krstić, V. V. Kovačević, A. Obrusník, Y. N. Nguyen, L. Zajíčková, B. M. Obradović, and M. M. Kuraica, Plasma Sources Sci. Technol. **25**, 065026 (2016).
[19]G. B. Sretenović, I. B. Krstić, V. V. Kovačević, B. M. Obradović, and M. M. Kuraica, J. Phys. D **47**, 355201 (2014).
[20]B. M. Obradović, S. S. Ivković, and M. M. Kuraica, Appl. Phys. Lett. **92**, 191501 (2008).
[21]M. M. Kuraica and N. Konjević, Appl. Phys. Lett. **70**, 1521 (1997).
[22]M. S. Simeni, Y. Zheng, E. V. Barnat, and P. J. Bruggeman, Plasma Sources Sci. Technol. **30**, 055004 (2021).
[23]G. B. Sretenović, I. B. Krstić, V. V. Kovačević, B. M. Obradović, and M. M. Kuraica, Appl. Phys. Lett. **99**, 161502 (2011).
[24]P. Viegas, E. Slikboer, Z. Bonaventura, O. Guaitella, A. Sobota, and A. Bourdon, Plasma Sources Sci. Technol. **31**, 053001 (2022).
[25]S. Djurović and N. Konjević, Plasma Sources Sci. Technol. **18**, 035011 (2009).
[26]N. V. Ivanović, N. M. Šišović, D. Spasojević, and N. Konjević, J. Phys. D **50**, 125201 (2017).
[27]N. V. Nedić, N. V. Ivanović, I. R. Videnović, D. Spasojević, and N. Konjević, J. Anal. At. Spectrom. **37**, 1318 (2022).
[28]Y. P. Raizer, *Gas Discharge Physics*, edited by J. E. Allen (Springer-Verlag, Berlin, Heidelberg, New-York, 1991).